

Atypical Sliding and Moiré Ferroelectricity in Pure Multilayer GrapheneLiu Yang¹, Shiping Ding¹, Jinhua Gao¹, and Menghao Wu^{1,2,*}¹*School of Physics, Huazhong University of Science and Technology, Wuhan 430074, China*²*School of Chemistry, Center of Theoretical Chemistry, Huazhong University of Science and Technology, Wuhan 430074, China* (Received 10 April 2023; accepted 21 July 2023; published 29 August 2023)

Most nonferroelectric two-dimensional materials can be endowed with so-called sliding ferroelectricity via nonequivalent homobilayer stacking, which is not applicable to mono-element systems like pure graphene bilayer with inversion symmetry at any sliding vector. Herein, we show first-principles evidence that multilayer graphene with $N > 3$ can all be ferroelectric, where the polarizations of polar states stem from the symmetry breaking in stacking configurations of across layer instead of adjacent layer, which are electrically switchable via interlayer sliding. The nonpolar states can also be electrically driven to polar states via sliding, and more diverse states with distinct polarizations will emerge in more layers. In contrast to the ferroelectric moiré domains with opposite polarization directions in twisted bilayers reported previously, the moiré pattern in some multilayer graphene systems (e.g., twisted monolayer-trilayer graphene) possess nonzero net polarizations with domains of the same direction separated by nonpolar regions, which can be electrically reversed upon interlayer sliding. The distinct moiré bands of two polar states should facilitate electrical detection of such sliding moiré ferroelectricity during switching.

DOI: [10.1103/PhysRevLett.131.096801](https://doi.org/10.1103/PhysRevLett.131.096801)

Ferroelectric crystals with switchable electrical polarizations are supposed to possess a lattice with certain breaking of symmetry. Such required symmetry breaking is absent in prevalent 2D materials like graphene, BN, and MoS₂ with highly symmetrical honeycomb lattices, which are thus nonferroelectric. In 2017 we proposed that for most 2D materials, vertical polarization can be induced in their bilayers and multilayers upon interlayer inequivalent stacking, which are switchable upon interlayer sliding (i.e., sliding ferroelectricity) driven by a vertical electric field, and a twist angle in such bilayer will give rise to a moiré pattern with periodic ferroelectric domains [1]. Within several years, such sliding ferroelectricity has been experimentally confirmed in a series of van der Waals bilayers and multilayers like BN [2–4], InSe [5], transition metal dichalcogenides including MoS₂ [6–11], WSe₂ [12,13], WTe₂ [14–16], MoTe₂ [17], ReS₂ [18], and even in amphidynamic crystals [19]. The ferroelectric moiré domains with opposite polarization directions have also been visualized in twisted BN [2,3,20] and MoS₂ [6,7] bilayers. In addition, mysterious ferroelectricity has been detected in twisted graphene/BN heterolayers [21–23]. Theoretically, a general group theory for bilayer sliding ferroelectricity [24], as well as models for estimating the Curie temperature [25,26] and the evolution ferroelectric moiré domains under an electric field have been proposed [27,28]. Such ferroelectricity can only be induced by certain stacking configurations, for example, parallel stacking for BN bilayer while its antiparallel configuration is nonpolar, which is not favorable for practical

applications since the formation of the latter phase is more common in fabrication and cannot be transformed to the former one simply via interlayer sliding.

However, a similar mechanism is not applicable to mono-element systems like pure graphene bilayer with inversion symmetry at any sliding vector, which is nonferroelectric upon any stacking configuration. In this Letter, we show that “more is different” for ferroelectricity in multilayer graphene. Our first-principles calculations reveal that pure graphene multilayers with layer number $N > 3$ will exhibit atypical sliding ferroelectricity, where the symmetry breaking can be induced by the stacking configurations of across layer (similar to the case in graphene/BN heterolayers [23]) instead of adjacent-layer, giving rise to a polarization that is electrically switchable via interlayer sliding. More layers with diversiform configurations give rise to various polar states with different polarizations, which can be used for multi-state memories [9,10] or even memristive-switching devices [29]. Herein all the polar and nonpolar states are interchangeable via sliding, averting the above-mentioned issue of forming stable nonpolar phase during fabrication.

The net polarization for ferroelectric moiré patterns of twisted homobilayers under zero electric field should be zero [27,28]. In comparison, we show that the moiré patterns of some twisted monolayer-multilayer graphene systems that have been realized previously [30] with alternating polar and nonpolar domains possess a nonzero net polarization electrically switchable via interlayer

sliding, which may be denoted as “sliding moiré ferroelectricity.” The distinct moiré bands of two polar states should lead to considerable difference in electron transport and thus facilitate experimental detection of its ferroelectric switching.

Density-functional-theory (DFT) calculations involved in this Letter were implemented in the Vienna *ab initio* simulation package (VASP5.4) code [31,32]. The projector augmented wave (PAW) potentials with the generalized gradient approximation in the Perdew-Burke-Ernzerhof [33] form were used to treat the electron-ion interactions. The DFT-D2 functional of Grimme [34] was used to describe the van der Waals interactions, and a large vacuum region with a thickness of 25 Å was added in the z direction to diminish interaction between adjacent slabs. The first Brillouin zone was sampled by the Monkhorst-Pack meshes method [35] with a $48 \times 48 \times 1$ k -point grid at the Γ center. The Gaussian smearing method was used with a smearing width 0.01 eV. The kinetic energy cutoff was set to be 520 eV and energy convergence criterion was set to 10^{-7} eV. The force convergence was set to be -10^{-3} eV/Å for the geometry optimization. The Berry phase method [36] was employed to evaluate the vertical polarization, and the ferroelectric switching pathways were obtained by using climbing image nudged elastic band (CI-NEB) method [37]. The band structures of the twisted moiré systems were calculated using the effective continuum model, with the same parameters in a previous study [38], while only the interlayer nearest-neighbor hopping is taken into account.

Graphene monolayer and bilayer (AB stacking as the ground state) are both nonpolar with centrosymmetry, as

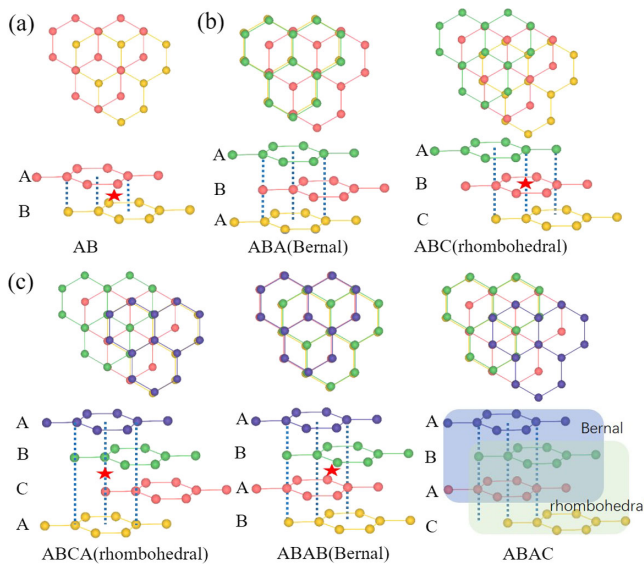


FIG. 1. Various stacking configurations of (a) bilayer, (b) trilayer, and (c) tetralayer graphene, where different layers are labeled in different colors and each red star denotes a center of inversion symmetry.

shown in Fig. 1. For the two configurations of trilayer graphene, neither Bernal stacking (ABA) with mirror symmetry nor rhombohedral stacking (ABC) with inversion symmetry possess a vertical polarization. For tetralayer graphene, similarly, rhombohedral ($ABCB$) and Bernal ($ABAB$) stacking with inversion symmetry are both nonpolar. However, in $ABAC$ stacking configuration which has been experimentally detected [39], such symmetry is broken by the across-layer configuration (AA stacking for the first through third layer and AB stacking for the second through fourth layer) albeit all the adjacent interlayer configurations are AB stacking. It is vice versa for another polar state $CABA$ (i.e., $ABCB$, AB stacking for the first through third layer and AA stacking for the second through fourth layer), as shown in Fig. 2(a), and their vertical polarizations are opposite as the two orientation states are correlated by mirror symmetry \hat{M}_{xy} . Meanwhile, this polar state $CABA$ and another polar state $CBAB$ (still AB stacking for the first through third layer and AA stacking for the second through fourth layer) are correlated by mirror symmetry \hat{M}_{yz} , so their in-plane polarizations are opposite. According to our calculations, the energy difference between those polar and nonpolar configurations are within 0.3 meV/unit cell. To our estimation by Berry phase method, those identical polar states possess a vertical polarization of 0.21 pC/m and a much higher in-plane polarization of 57.49 pC/m (5.93 $\mu\text{C}/\text{cm}^2$ in 3D unit) in different orientations. Their dynamical stability and thermal stability are confirmed by the phonon spectrum free of imaginary frequency and the snapshot of molecular dynamics simulation in Fig. S1 [40]. Our simulated STM images in Fig. S2 [40] can also differentiate the polar states from nonpolar states.

We note that all the transformation between those configurations can simply be achieved by shear displacement, i.e., interlayer sliding. For example, $ABAC$ can be transformed into $ABCB$ via the simultaneous translation of the two down layers by a $C-C$ bond length. Meanwhile, for the transition pathway between $ABAC$ and $CBAB$ states, either of the nonpolar $ABAB$ and $CBAC$ states can be the intermediate state. As shown in Fig. 2(b), in pathway I, the $ABAC$ state can transform into the $ABAB$ state via the sliding of the fourth layer, and then into the $CBAB$ state via the sliding of the first layer. In path II, the $ABAC$ state can transform into the $CBAC$ state via the sliding of the first layer, and then into the $CBAB$ state via the sliding of the fourth layer. Such switching barriers are both lower than the 5 meV/unit cell according to our NEB calculations, so the polarizations can be reversibly switched. For the nonpolar $CBAC$ and $ABAB$ states, they can also be electrically transformed to the polar $CBAB$ or $ABAC$ state via the translation of the first or fourth layer, depending on the direction of external electric field.

The origin of vertical polarizations can be further clarified by the charge distributions in Fig. 2(c) that show the evidence of nonequivalence between the second and

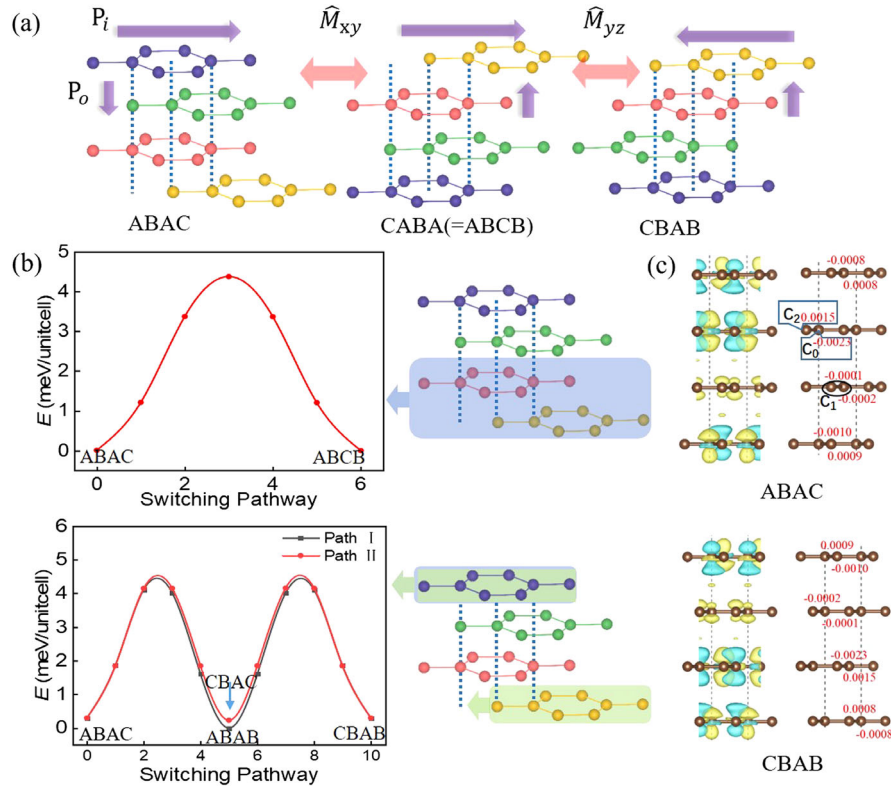


FIG. 2. (a) Transformation between the polar states *ABAC*, *CABA*, and *CBAB*, and (b) the corresponding switching pathway calculated by NEB methods, where the polarization directions are denoted by purple arrows. (c) The differential charge density distributions of polar states and Hirshfeld charge analysis, where yellow and blue isosurfaces, respectively, indicate electron accumulation and depletion after layer stacking.

third layer with distinct distribution of π electron clouds. The Hirshfeld charge analysis can also provide insight into the breaking of symmetry and the interlayer charge transfer. The charges on the second and third graphene are, respectively, -0.0008 and $-0.0003e$ per unit cell for *ABAC* stacking, which is vice versa for *CBAB* stacking. For the second and third layer in the center, we denote the carbon atom right between two C atoms of adjacent layers at two sides as C_2 , the carbon atom right between two hexagon centers of adjacent layers at two sides as C_0 , and the carbon atom only over one C atom at one side as C_1 . It turns out that each C_0 , C_1 , and C_2 atom, respectively, carries a charge of $-0.0023e$, $-0.0001e$, and $0.0015e$ so the different environment of two carbon layers may be the origin of their different electron distribution. The vertical polarization induced by the nonsymmetric charge distribution should be detectable by using an atomic force microscope in a side-band Kelvin probe mode to measure the surface potential, noting that the ferroelectric domains of sliding ferroelectric systems have been visualized by similar techniques in previous experimental reports [3,10].

Similar ferroelectric mechanism can be applied to more layers with various polar states. For the stacking configurations of five layers displayed in Fig. 3(a), their

differences are within 0.4 meV/unit cell, in which *ABABC* and *ABACB* are polar states with a vertical polarization of 0.17 and 0.32 pC/m, respectively, while other states are nonpolar. The stacking configurations become much more complicated for six layers, where the energy differences between multiple states in Fig. 3(b) are within 0.6 meV/unit cell, and the vertical polarizations of five polar states ranging approximately from 0.05 to 1.0 pC/m may render multibit memories [9,10] possible. For more layers with much more possible stacking configurations, the number of diversiform polar states may even be enough for memristive-switching devices [29]. Distinct from previously reported bilayer ferroelectric systems, the parallel and antiparallel stacking configurations are the same for graphene multilayers, so all their stacking configurations are interchangeable simply via interlayer sliding. The general principle to judge the existence of ferroelectricity in various stacking configurations for graphene multilayers is also much simpler: they are ferroelectric if neither \hat{I} nor \hat{M}_{xy} symmetry exist.

For the moiré ferroelectric domains with staggered polarizations induced by a small twist angle in sliding ferroelectric bilayers (e.g., parallel stacking BN bilayer), it has already been revealed both experimentally [2,7] and theoretically [27,28] that the coupling between the spontaneous

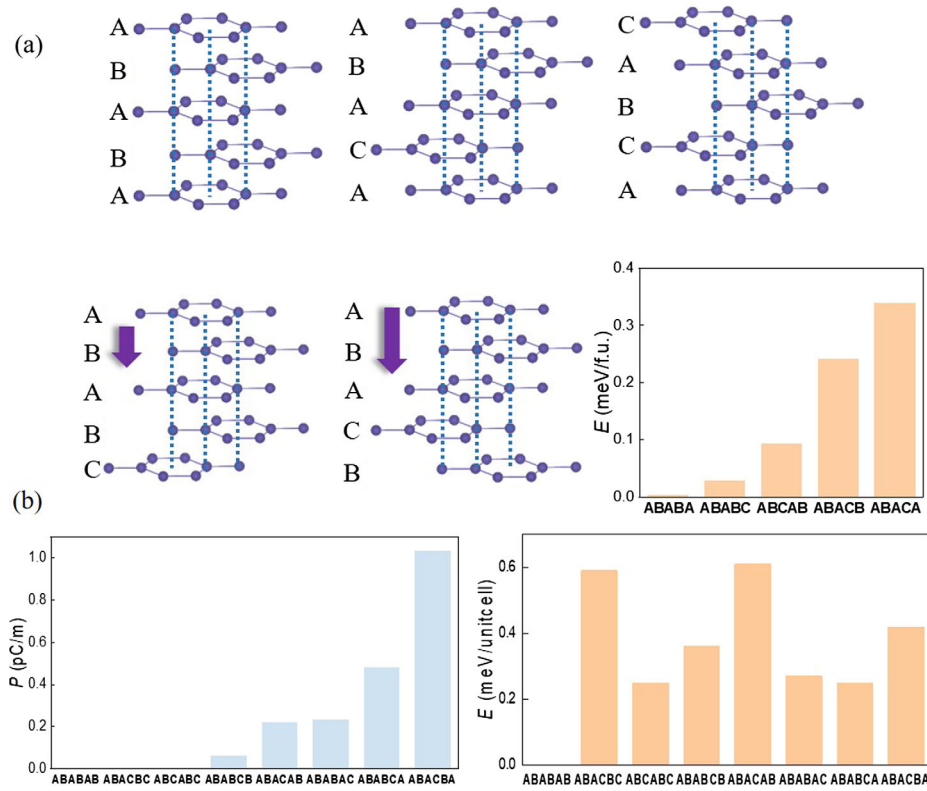


FIG. 3. (a) Various stacking configurations of five-layer graphene, where *ABABC* and *ABACB* are polar states with distinct vertical polarizations, but negligible difference in energy according to the energy diagram of different states. (b) Diagrams of vertical polarizations and relative energy for the various stacking configurations of six-layer graphene.

polarization and field leads to uneven relaxation of moiré ferroelectric domains, and a net polarization in the superlattice at nonzero field. Without an electric field, however, nonzero polarization is not supposed to form spontaneously in those moiré systems. In a twisted graphene bilayer, even the local polarization should be absent due to the local symmetry. For a four-layer graphene with a twist angle located in the center, i.e., between the upper second layer and third layer, which is previously referred to as the twisted double bilayer graphene (“2 + 2”), as shown in Fig. 4(a), it can be either twisted *AB-AB* stacking or *AB-BA* stacking. Herein, the regions containing *AA* stacking of adjacent layers will be contracted to small areas by atomic reconstruction due to their high energy compared with *AB* stacking. As a result, the twisted *AB-AB* stacking tetralayer graphene will be mainly occupied by two nonpolar (NP) domains of *ABAB* and *BCAB*. For the twisted *AB-BA* stacking configurations, the two coexisting ferroelectric domains *BCBA* and *CABA* with opposite polarizations should yield a zero net polarization.

If the twist angle is located between the first and second layer, in such twisted monolayer-trilayer (1 + 3) graphene, the trilayer graphene can be either *ABA* or *ABC* stacking. In the former case, e.g., monolayer on a Bernal stacked trilayer graphene, triangular domains of two reconstruction states *BABA* and *CABA* will be formed,

as shown in Fig. 4(b). Herein, the *BABA* state is nonpolar while the *CABA* state is polar with a vertical polarization around 0.21 pC/m, so the overall twisted system possesses a nonzero vertical polarization even without an electric field. In such a twisted system, the *BABA* domains cannot be transformed to *CABA* domains via the translation of the first layer, or the adjacent *CABA* domain will be simultaneously transformed to unfavorable *AABA* domains upon the same interlayer translation vector. When a reversed electrical field is applied to the twisted system, as shown in Fig. 4(c), the polar *CABA* domains may be transformed to nonpolar *CABC* domains upon the translation of the bottom layer, while the nonpolar *BABA* domains will become *BABC* domains (equivalent to *CABA* albeit with opposite polarizations of 0.21 pC/m). As a result, the net polarization of the whole twisted graphene system can be reversed via interlayer sliding, and such “sliding moiré ferroelectricity” is distinct from previous reported moiré ferroelectricity [2,7] where the altering of net polarization under an electric field is induced by the lattice relaxation changing the domains. Similar ferroelectricity may be further applicable to many other twisted multilayer systems with more layers, also mainly occupied by domains of two states with different polarizations, which will be transformed to two other states upon interlayer sliding.

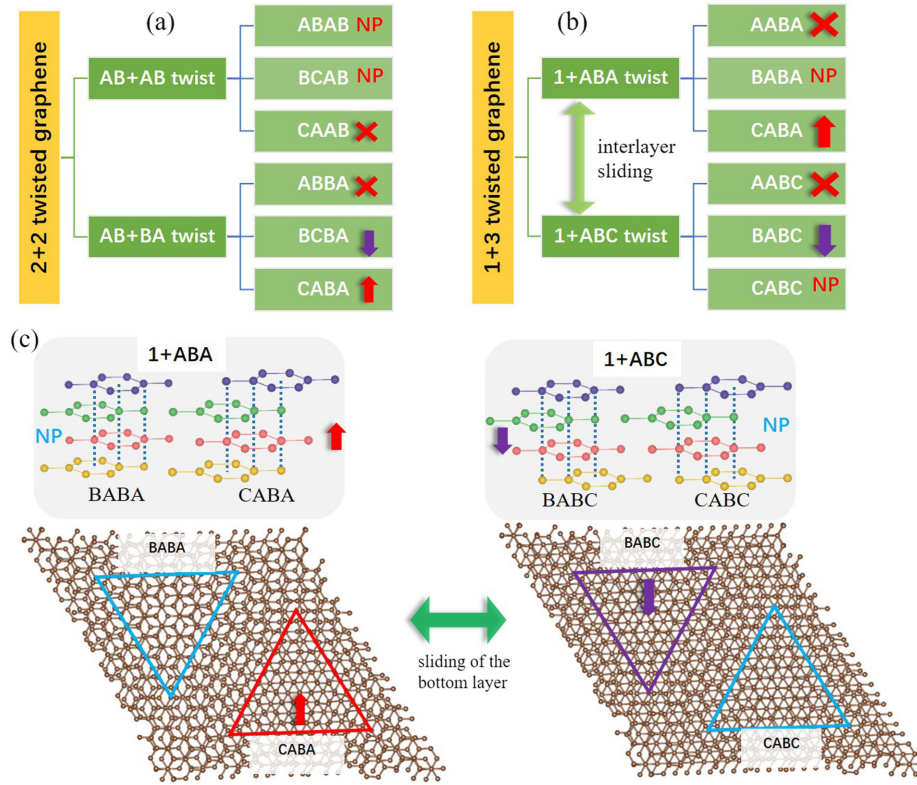


FIG. 4. Different stacking domains of (a) 2 + 2 and (b) 1 + 3 twisted tetralayer graphene, where the arrows denote polarization directions, NP and X, respectively, indicate that the domain is nonpolar and unfavorable in energy. (c) Bipolar states of 1 + 3 twisted tetralayer graphene and ferroelectric switching pathway.

Finally, the band structures of those tetralayer graphene systems are investigated. All the band structures of the three nontwisted stacking configurations in Fig. 1(c) exhibit four pairs of massive bands [see Fig. 5(a)], with obvious differences near the Fermi level at the K point. For the $CABC$ stacking, a pair of nearly dispersionless flat bands are localized around the K point near the Fermi level, while two pairs of twofold-degenerate bands in $ABAB$ stacking configuration cross the Fermi level, so both nonpolar systems are metallic. For the polar $ABAC$ stacking configuration, the electronic structure near the Fermi level around the K points is characterized by two pairs of low-energy bands, including a pair of linearly dispersed bands and a pair of localized flat bands, giving rise to a band gap around 12 meV. The opening of the band gap may solve the long-standing metallic behavior issue of few-layer graphene, which can be attributed to the vertical polarization and built-in electric field induced by the nonsymmetric charge distribution. Those results are in accord with previous studies [41,42], making the polar and nonpolar states electrically differentiable in experiments.

We also calculate the band structures of twisted monolayer-trilayer graphene $1 + ABA$ and $1 + ABC$ with opposite polarizations using the effective continuum model,

where the twist angle is set to be 1.08° . In the band structure of $1 + ABA$ shown in Fig. 5(b), a pair of flat bands near the Fermi level coexist with a pair of linear bands crossing the Fermi level at the K point. However, such linear bands are missing in the band structure of $1 + ABC$ shown in Fig. 5(c), leaving only a pair of flat bands near the Fermi level. The differences in low-energy energy spectra of these systems are consistent with the generic partitioning rules [43] as well as previous calculations on twisted multilayer graphene [44–49], which should lead to a detectable difference in electrical transport measurement during ferroelectric switching.

In summary, we propose an abnormal type of sliding ferroelectricity where the symmetry breaking is induced by the stacking configurations of across-layer instead of adjacent-layer, and demonstrate its existence in tetralayer graphene. It also exists in more layers with more diversified states of different polarizations, which can be used for multistate memories. We also predict the so-called sliding moiré ferroelectricity in some twisted monolayer-multilayer graphene systems with alternating polar and nonpolar domains, with a nonzero net polarization electrically switchable via interlayer sliding. Our predictions of those hitherto unreported types of ferroelectricity are all based on simple pure graphene systems and should

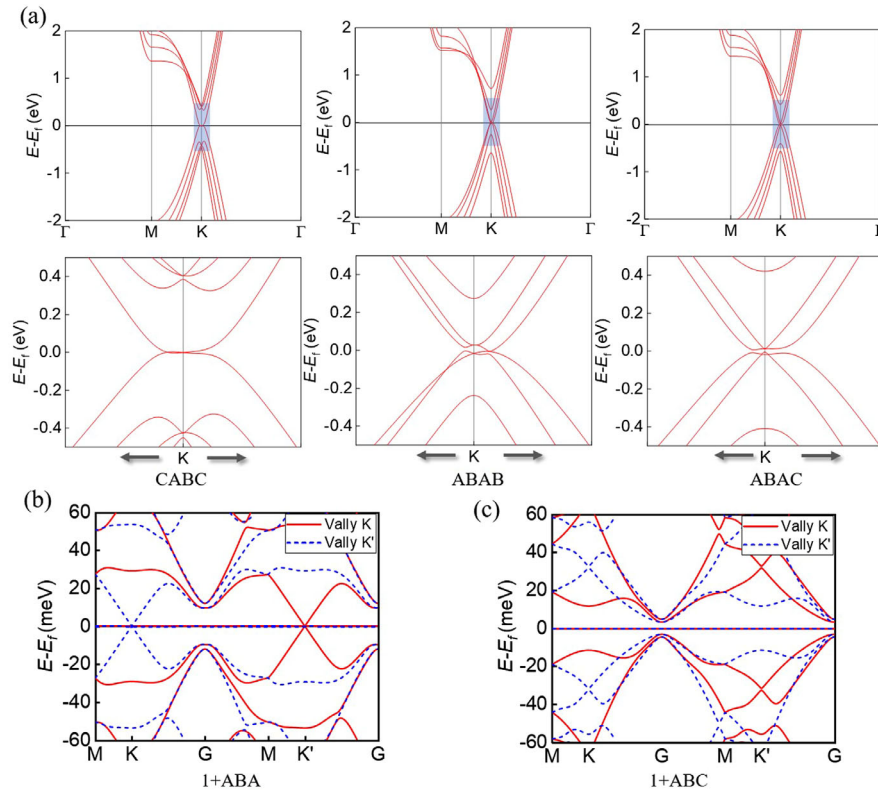


FIG. 5. The band structures of (a) untwisted, (b) $1 + ABA$, and (c) $1 + ABC$ twisted tetralayer graphene, where bands of valley K and K' in twisted systems are shown as solid and dashed lines, respectively.

stimulate experimental efforts in the future, noting that another ferroelectric monoelement system has been recently confirmed [50].

This work is supported by the National Natural Science Foundation of China (No. 22073034).

L. Y., S. D., and J. G. contributed equally to the work.

Note added.—During the review of our manuscript, we note that theoretical and experimental results supporting some of our findings were reported in two other works [51,52].

*Corresponding author: wmh1987@hust.edu.cn

- [1] L. Li and M. Wu, *ACS Nano* **11**, 6382 (2017).
- [2] K. Yasuda, X. Wang, K. Watanabe, T. Taniguchi, and P. Jarillo-Herrero, *Science* **372**, 1458 (2021).
- [3] M. Vizner Stern, Y. Waschitz, W. Cao, I. Nevo, K. Watanabe, T. Taniguchi, E. Sela, M. Urbakh, O. Hod, and M. Ben Shalom, *Science* **372**, 1462 (2021).
- [4] M. Lv, X. Sun, Y. Chen, T. Taniguchi, K. Watanabe, M. Wu, J. Wang, and J. Xue, *Adv. Mater.* **34**, 2203990 (2022).
- [5] F. Sui, M. Jin, Y. Zhang, R. Qi, Y.-N. Wu, R. Huang, F. Yue, and J. Chu, *Nat. Commun.* **14**, 36 (2023).
- [6] A. Weston *et al.*, *Nat. Nanotechnol.* **17**, 390 (2022).
- [7] X. Wang, K. Yasuda, Y. Zhang, S. Liu, K. Watanabe, T. Taniguchi, J. Hone, L. Fu, and P. Jarillo-Herrero, *Nat. Nanotechnol.* **17**, 367 (2022).

- [8] L. Rogée, L. Wang, Y. Zhang, S. Cai, P. Wang, M. Chhowalla, W. Ji, and S. P. Lau, *Science* **376**, 973 (2022).
- [9] P. Meng *et al.*, *Nat. Commun.* **13**, 7696 (2022).
- [10] S. Deb, W. Cao, N. Raab, K. Watanabe, T. Taniguchi, M. Goldstein, L. Kronik, M. Urbakh, O. Hod, and M. B. Shalom, *Nature (London)* **612**, 465 (2022).
- [11] A. Lipatov *et al.*, *npj 2D Mater. Appl.* **6**, 18 (2022).
- [12] Y. Liu, S. Liu, B. Li, W. J. Yoo, and J. Hone, *Nano Lett.* **22**, 1265 (2022).
- [13] Y. Sun *et al.*, *Nat. Commun.* **13**, 5391 (2022).
- [14] Z. Fei, W. Zhao, T. A. Palomaki, B. Sun, M. K. Miller, Z. Zhao, J. Yan, X. Xu, and D. H. Cobden, *Nature (London)* **560**, 336 (2018).
- [15] P. Sharma, F.-X. Xiang, D.-F. Shao, D. Zhang, E. Y. Tsymlar, A. R. Hamilton, and J. Seidel, *Sci. Adv.* **5**, eaax5080 (2019).
- [16] S. C. de la Barrera, Q. Cao, Y. Gao, Y. Gao, V. S. Bheemarasetty, J. Yan, D. G. Mandrus, W. Zhu, D. Xiao, and B. M. Hunt, *Nat. Commun.* **12**, 5298 (2021).
- [17] A. Jindal *et al.*, *Nature (London)* **613**, 48 (2023).
- [18] Y. Wan *et al.*, *Phys. Rev. Lett.* **128**, 067601 (2022).
- [19] L. P. Miao, N. Ding, N. Wang, C. Shi, H. Y. Ye, L. L. Li, Y. F. Yao, S. Dong, and Y. Zhang, *Nat. Mater.* **21**, 1158 (2022).
- [20] C. R. Woods, P. Ares, H. Nevison-Andrews, M. J. Holwill, R. Fabregas, F. Guinea, A. K. Geim, K. S. Novoselov, N. R. Walet, and L. Fumagalli, *Nat. Commun.* **12**, 347 (2021).
- [21] Z. Zheng *et al.*, *Nature (London)* **588**, 71 (2020).
- [22] R. Niu *et al.*, *Nat. Commun.* **13**, 6241 (2022).
- [23] L. Yang and M. Wu, *Adv. Funct. Mater.* **33**, 01105 (2023).
- [24] J. Ji, G. Yu, C. Xu, and H. J. Xiang, *Phys. Rev. Lett.* **130**, 146801 (2023).

- [25] J. M. Marmolejo-Tejada, J. E. Roll, S. P. Poudel, S. Barraza-Lopez, and M. A. Mosquera, *Nano Lett.* **22**, 7984 (2022).
- [26] P. Tang and G. E. W. Bauer, *Phys. Rev. Lett.* **130**, 176801 (2023).
- [27] D. Bennett and B. Remez, *npj 2D Mater. Appl.* **6**, 7 (2022).
- [28] V. V. Enaldiev, F. Ferreira, and V. I. Fal'ko, *Nano Lett.* **22**, 1534 (2022).
- [29] M. Rao *et al.*, *Nature (London)* **615**, 823 (2023).
- [30] S. Zhang *et al.*, *Nat. Mater.* **21**, 621 (2022).
- [31] G. Kresse and J. Furthmüller, *Phys. Rev. B* **54**, 11169 (1996).
- [32] G. Kresse and J. Furthmüller, *Comput. Mater. Sci.* **6**, 15 (1996).
- [33] J. P. Perdew, K. Burke, and M. Ernzerhof, *Phys. Rev. Lett.* **77**, 3865 (1996).
- [34] S. Grimme, *J. Comput. Chem.* **27**, 1787 (2006).
- [35] H. J. Monkhorst and J. D. Pack, *Phys. Rev. B* **13**, 5188 (1976).
- [36] R. D. King-Smith and D. Vanderbilt, *Phys. Rev. B* **47**, 1651 (1993).
- [37] G. Henkelman, B. P. Uberuaga, and H. Jónsson, *J. Chem. Phys.* **113**, 9901 (2000).
- [38] M. Koshino, N. F. Q. Yuan, T. Koretsune, M. Ochi, K. Kuroki, and L. Fu, *Phys. Rev. X* **8**, 031087 (2018).
- [39] K. G. Wirth *et al.*, *ACS Nano* **16**, 16617 (2022).
- [40] See Supplemental Material at <http://link.aps.org/supplemental/10.1103/PhysRevLett.131.096801> for the phonon spectrum, molecular dynamics simulation, and simulated STM images of tetralayer graphene.
- [41] K. F. Mak, J. Shan, and T. F. Heinz, *Phys. Rev. Lett.* **104**, 176404 (2010).
- [42] S. Latil and L. Henrard, *Phys. Rev. Lett.* **97**, 036803 (2006).
- [43] S. Zhang, B. Xie, Q. Wu, J. Liu, and O. V. Yazyev, *Nano Lett.* **23**, 2921 (2023).
- [44] N. R. Chebrolu, B. L. Chittari, and J. Jung, *Phys. Rev. B* **99**, 235417 (2019).
- [45] M. Liang, M.-M. Xiao, Z. Ma, and J.-H. Gao, *Phys. Rev. B* **105**, 195422 (2022).
- [46] J. Liu, Z. Ma, J. Gao, and X. Dai, *Phys. Rev. X* **9**, 031021 (2019).
- [47] Z. Ma, S. Li, M.-M. Xiao, Y.-W. Zheng, M. Lu, H. Liu, J.-H. Gao, and X. C. Xie, *Front. Phys.* **18**, 13307 (2022).
- [48] J. Cao, M. Wang, S.-F. Qian, C.-C. Liu, and Y. Yao, *Phys. Rev. B* **104**, L081403 (2021).
- [49] W. Wang, Y. Shi, A. A. Zakharov, M. Syväjärvi, R. Yakimova, R. I. G. Uhrberg, and J. Sun, *Nano Lett.* **18**, 5862 (2018).
- [50] J. Gou, H. Bai, X. Zhang, Y. L. Huang, S. Duan, A. Ariando, S. A. Yang, L. Chen, Y. Lu, and A. T. S. Wee, *Nature (London)* **617**, 67 (2023).
- [51] A. Garcia-Ruiz, V. Enaldiev, A. McEllistrim, and V. I. Fal'ko, *Nano Lett.* **23**, 4120 (2023).
- [52] S. S. Atri *et al.* [arXiv:2305.10890](https://arxiv.org/abs/2305.10890).